In memory of T. A. Stephenson

Diplatinum-(II) and -(III) Complexes with Bridging μ-Diphosphonito-*P,P'* or μ-Methylenebis(phosphonito)-*P,P'* Ligands. Synthesis, Structure, and Nuclear Magnetic Resonance Analysis of the 'Lantern' Complexes. Crystal Structures of $K_4[Pt_2\{\mu\text{-}CH_2[P(O)OH]_2\}_4]\cdot 6H_2O$ and $K_4[Pt_2\{\mu\text{-}CH_2[P(O)OH]_2\}_4Cl_2]\cdot 8H_2O$†

Christopher King and D. Max Roundhill *
Department of Chemistry, Tulane University, New Orleans, Louisiana 70118, U.S.A.
Mark K. Dickson
Department of Chemistry, Washington State University, Pullman, Washington 99164, U.S.A.
Frank R. Fronczek
Department of Chemistry, Louisiana State University, Baton Rouge, Louisiana 70803, U.S.A.

The complex $K_4[Pt_2\{\mu\text{-}CH_2[P(O)OH]_2\}_4]\cdot 6H_2O$ $\{K_4[Pt_2(pcp)_4]\}$ has been prepared by treating $K_2[PtCl_4]$ with $CH_2[PH(O)OH]_2$. The structure shows a 'lantern' arrangement of phosphorus ligands about the two platinum(II) centres, with a Pt–Pt separation of 2.980 1(2) Å. This complex, $K_4[Pt_2(pcp)_4]$, reacts with halogens X_2 (X = Cl, Br, or I) to give diplatinum(III) complexes $K_4[Pt_2(pcp)_4X_2]$ The structure of the dichloro complex $K_4[Pt_2\{\mu\text{-}CH_2[P(O)OH]_2\}_4Cl_2]\cdot 8H_2O$ shows long Pt–Cl distances of 2.442(1) Å and a short Pt–Pt separation of 2.750 0(3) Å. The complexes $[Pt_2(pcp)_4X_2]^{4-}$ show $X\rightarrow Pt^{III}$ ligand to metal charge transfer bands at 298 (X = Cl), 326 (X = Br), 354 and 454 nm (X = I). The $^{31}P\text{-}\{^1H\}$ and $^{195}Pt\text{-}\{^1H\}$ n.m.r. spectra of the complexes $[Pt_2(pcp)_4]^{4-}$, $[Pt_2(pcp)_4X_2]^{4-}$, $[Pt_2(pop)_4]^{4-}$, and $[Pt_2(pop)_4X_2]^{4-}$ {X = Cl, Br, or I; pop = $\mu\text{-}O[P(O)OH]_2^{2-}$} have been solved by second-order analysis of the nine-spin $Pt^{195}Pt$ and ten-spin $^{195}Pt_2$ isotopomer mixtures in the solutions. The spectra have been simulated as the $[A_4][X]_2[A'_4]$ spin system using the program PANIC, and as the $[A]_4[X]_2[A']_4$ spin system using DSYMPLOT. In the diplatinum(II) complexes $^1J(PtPt) < 1\,000$ Hz, but in the diplatinum(III) complexes $^1J(PtPt) \approx 7\,000$—$11\,000$ Hz.

The binuclear complex $[Pt_2(pop)_4]^{4-}$ {pop, diphosphonite = $\mu\text{-}O[P(O)OH]_2^{2-}$} has attracted interest because of its intense luminescence in aqueous solution.[1] The complex has a 'lantern' structure with the four μ-diphosphonito groups bonded to platinum(II) through the phosphorus atoms.[2] In a preliminary communication[3] we reported that the addition of halogen (X_2) to this complex leads to the formation of axially substituted halogenodiplatinum(III) complexes $[Pt_2(pop)_4X_2]^{4-}$ (X = Cl, Br, or I).[4] Analysis of differences in intermetallic bond lengths and force constants[5] between the complexes $[Pt_2(pop)_4]^{4-}$ and $[Pt_2(pop)_4X_2]^{4-}$ indicates that there is minimal bonding between the platinum atoms in $[Pt_2(pop)_4]^{4-}$, but that in the complexes $[Pt_2(pop)_4X_2]^{4-}$ there is a single bond between the platinum atoms.

In previous papers[6,7] we have reported that the compound $CH_2[PH(O)OH]_2$ can be used to prepare the analogous diplatinum(II) 'lantern' complex $[Pt_2(pcp)_4]^{4-}$ {pcp = $\mu\text{-}CH_2[P(O)OH]_2^{2-}$} and the photophysical properties of $[Pt_2(pop)_4]^{4-}$ and $[Pt_2(pcp)_4]^{4-}$ were found to be analogous, except for the triplet state lifetime of $[Pt_2(pcp)_4]^{4-}$ being shorter at ambient temperature. In this paper we now describe the synthetic details for the preparation of $[Pt_2(pcp)_4]^{4-}$, along with the formation of aqueous solutions of the diplatinum(III) complexes $[Pt_2(pop)_4X_2]^{4-}$ and $[Pt_2(pcp)_4X_2]^{4-}$ (X = Cl, Br, or I). Finally, we use a combination of ^{31}P and ^{195}Pt n.m.r. spectroscopy to assess intermetallic bonding differences between the diplatinum(II) and diplatinum(III) sets of complexes. These n.m.r. spectral analyses cannot be carried out by simple first-order methods since the aqueous solutions of individual complexes contain mixtures of the three isotopomers Pt_2, $Pt^{195}Pt$, and $^{195}Pt_2$, with the latter two sets of complexes having nine-spin $[A]_4[X][A']_4$ and ten-spin $[A]_4[X]_2[A']_4$ systems respectively.

Experimental

The complex $K_4[Pt_2(pop)_4]\cdot 2H_2O$ was prepared by the literature procedure,[8] as was the compound $CH_2[PH(O)OH]_2$ (H_2pcp).[6] U.v.—visible spectra were recorded on a Hewlett-Packard model 8451A spectrophotometer. Potassium tetrachloroplatinate was purchased from Johnson Matthey, Inc. Analyses were performed by Canadian Microanalytical Services, Vancouver, B.C. or by Galbraith Laboratories, Knoxville, Tennessee. Solution n.m.r. spectra were collected with samples dissolved in D_2O solvent in 12-mm or 10-mm tubes. Data with the 12-mm tubes were collected on a Nicolet NT 200 spectrometer, and those with the 10-mm tubes on a Bruker AC 200 spectrometer. The $^{31}P\text{-}\{^1H\}$ and $^{195}Pt\text{-}\{^1H\}$ spectra were collected using two-level decoupling to prevent solvent heating. Phosphorus-31 spectra were referenced to external H_3PO_4, and ^{195}Pt spectra to external H_2PtCl_6. Representative data collection used a 30° pulse angle with acquisition times of 0.8—4.0 s for ^{31}P and 0.2 s for ^{195}Pt spectra, or an 80° pulse angle for ^{195}Pt spectra with an acquisition time of 0.4 s. The T_1 values of

† Potassium tetra[μ-methylenebis(phosphonito)-*P,P'*]-diplatinate(II) hexahydrate and potassium dichlorotetra[μ-methylenebis(phosphonito)-*P,P'*]-diplatinate(III)(*Pt–Pt*) octahydrate.

Supplementary data available: see Instructions for Authors, *J. Chem. Soc., Dalton Trans.*, 1987, Issue 1, pp. xvii—xx.

0.21(1) and 0.28(4) s for the ^{195}Pt resonances were measured for $[Pt_2(pcp)_4]^{4-}$ and $[Pt_2(pop)_4]^{4-}$ respectively using an inversion recovery method on aqueous solutions of the complexes purged with nitrogen. The spectra of $[Pt_2(pcp)_4]^{4-}$ for T_1 measurement were collected with broad-band proton decoupling of the methylenic protons.

Syntheses.—$K_4[Pt_2\{\mu\text{-}CH_2[P(O)OH]_2\}_4]\cdot 6H_2O$. Potassium tetrachloroplatinate (0.1 g), $K_2(pcp)$ (0.21 g), and potassium acetate (0.3 cm^3 of 1 mol dm^{-3} CH_3CO_2H adjusted to pH 5 with KOH) were heated for 72 h at 103 °C in a glass tube (8 mm × 40 mm) which was flushed with nitrogen and sealed with a septum. The yellow crystals of the product which formed were manually separated. Addition of ethyl alcohol to the supernatant liquid gave additional product. This material was filtered off and dried *in vacuo* for 3 d. Yield of isolated product 60—70% (>95% purity by $^{31}P\text{-}\{^1H\}$ n.m.r. spectroscopy) (Found: C, 3.95; H, 2.15. $C_4H_{28}K_4O_{22}P_8Pt_2$ requires C, 3.95; H, 2.30%).

$K_4[Pt_2\{\mu\text{-}O[P(O)OH]_2\}_4Cl_2]$. Chlorine gas was passed slowly through a deoxygenated aqueous solution (*ca.* 5 cm^3) of $K_4[Pt_2(pop)_4]\cdot 2H_2O$ (0.5 g, 1.2 mmol) for 20 min. The solution immediately changed colour to yellow due to loss of the 514-nm emission from $[Pt_2(pop)_4]^{4-}$. Slow addition of ethyl alcohol or acetonitrile to the solution gave a bright yellow powder which was washed with ethyl alcohol, and dried *in vacuo* for 12 h. Yield 60—70% (Found: Cl, 7.2; P, 19.5. $H_8Cl_2K_4O_{20}P_8Pt_2$ requires Cl, 5.9; P, 20.8%).

$K_4[Pt_2\{\mu\text{-}O[P(O)OH]_2\}_4Br_2]\cdot 4H_2O$. An excess of liquid bromine was added directly to a deoxygenated aqueous solution (*ca.* 5 cm^3) of $K_4[Pt_2(pop)_4]\cdot 2H_2O$ (0.5 g, 1.2 mmol). The solution, which immediately changed colour to orange, was stirred for 45 min. Slow addition of ethyl alcohol gave an orange powder which was filtered off, washed with ethyl alcohol, and dried *in vacuo* for 12 h. Yield 70—80% (Found: Br, 11.2; P, 18.6. $H_{16}Br_2K_4O_{24}P_8Pt_2$ requires Br, 11.8; P, 18.3%).

$K_4[Pt_2\{\mu\text{-}O[P(O)OH]_2\}_4I_2]$. Excess of iodine was added to a deoxygenated aqueous solution (*ca.* 5 cm^3) of $K_4[Pt_2(pop)_4]\cdot 2H_2O$ (0.5 g, 1.2 mmol). A deep red-brown colour appeared. Slow addition of ethyl alcohol, methyl alcohol, or acetonitrile produced a red-brown powder which was dried *in vacuo* for 12 h. Yield 70—75% (Found: I, 18.6; P, 17.7. $H_8I_2K_4O_{20}P_8Pt_2$ requires I, 18.4; P 18.0%).

The analytical data for the complexes $K_4[Pt_2\{\mu\text{-}O[P(O)OH]_2\}_4X_2]$ (X = Cl, Br, or I) are not entirely satisfactory, although the high purity of the compounds is supported by the ^{31}P n.m.r. spectra of their aqueous solutions which show no significant phosphorus-containing impurities.

$K_4[Pt_2\{\mu\text{-}CH_2[P(O)OH]_2\}_4Cl_2]$. Solutions of this complex suitable for n.m.r. analysis were prepared by syringe injection of a small quantity of chlorine into a nitrogen stream bubbling through ice-cold solutions of $K_4[Pt_2(pcp)_4]$ in D_2O solvent, followed by purging with nitrogen to remove excess of chlorine. Addition of excess of chlorine was avoided. The progress of the reaction was followed both by monitoring changes in the ^{31}P n.m.r. spectrum and by observing the loss (at 77 K) of the phosphorescence due to $[Pt_2(pcp)_4]^{4-}$.

$K_4[Pt_2\{\mu\text{-}CH_2[P(O)OH]_2\}_4Br_2]$. Using a similar procedure as for $[Pt_2(pcp)_4Cl_2]^{4-}$, except that bromine vapour was now added to the nitrogen stream by passing the carrier gas over bromine liquid, solutions of this complex in D_2O were prepared. Addition of excess of bromine was avoided.

$K_4[Pt_2\{\mu\text{-}CH_2[P(O)OH]_2\}_4I_2]$. Small aliquots of an aqueous solution containing iodine and sodium iodide were added to an aqueous solution of $K_4[Pt_2(pcp)_4]$ cooled to 0 °C. When the reaction was complete, as determined by ^{31}P n.m.r. spectroscopy, the complex was precipitated as a red powder by addition of acetone.

X-Ray Crystal-structure Analysis of $K_4[Pt_2(pcp)_4]\cdot 6H_2O$ *and* $K_4[Pt_2(pcp)_4Cl_2]\cdot 8H_2O$.—A crystal of $K_4[Pt_2\{\mu\text{-}CH_2[P(O)OH]_2\}_4]\cdot 6H_2O$ was grown directly according to the

Table 1. Crystal and intensity data collection summary

Formula	$K_4[Pt_2\{\mu\text{-}CH_2[P(O)OH]_2\}_4]\cdot 6H_2O$	$K_4[Pt_2\{\mu\text{-}CH_2[P(O)OH]_2\}_4Cl_2]\cdot 8H_2O$
M	1 222.7	1 329.6
Colour	Yellow-green	Red
a/Å	12.708(1)	9.179(2)
b/Å	12.429(1)	9.788(3)
c/Å	9.555(2)	10.625(2)
α/°		68.83(2)
β/°	93.57(2)	81.35(2)
γ/°		75.17(2)
U/Å^3	1 506.2(7)	858.7(4)
Crystal system	Monoclinic	Triclinic
Space group	$P2_1/n$	$P\bar{1}$
Z	2	1
D_c/g cm^{-3}	2.696	2.571
Crystal dimensions/mm	0.14 × 0.16 × 0.34	0.14 × 0.15 × 0.24
μ/cm^{-1}	104.3	93.1
$F(000)$	1 160	634
Temp/°C	20	25
Min. rel. transmission (%)	77.67	78.97
θ limits/°	1—32	1.0—25.0 (some 25.0—27.0)
Reflections	$h, k, \pm l$	$h, \pm k, \pm l$
No. of unique reflections	5 219	3 541
Reflections with ($F_o^2 > 3\sigma$)	4 442	3 194
$R(F)$[a]	0.021	0.023
$R'(F)$[b]	0.026	0.031
No. of variables	214	200
Max. residual (e Å^{-3})	0.87 (near Pt)	0.93 (near Pt)

[a] $R = \Sigma||F_o| - |F_c||/\Sigma|F_o|$. [b] $R' = [\Sigma w(|F_o| - |F_c|)^2/\Sigma wF_o^2]^{\frac{1}{2}}$; $w = 4F_o^2[\sigma^2(I) + (0.02F_o^2)^2]^{-1}$.

Table 2. Final atomic co-ordinates for $K_4[Pt_2\{\mu\text{-}CH_2[P(O)OH]_2\}_4]\cdot 6H_2O$

Atom	x	y	z	Atom	x	y	z
Pt	0.091 42(1)	0.060 11(1)	0.066 54(1)	O(4)	0.040 4(2)	−0.165 9(2)	−0.323 0(2)
K(1)	0.769 33(5)	0.107 64(6)	0.421 44(7)	O(5)	0.099 7(2)	0.021 8(2)	0.404 9(2)
K(2)	−0.004 98(8)	0.529 47(8)	0.281 44(10)	O(6)	0.180 6(2)	−0.130 6(2)	0.286 6(2)
P(1)	0.212 03(6)	−0.055 87(6)	−0.028 80(8)	O(7)	−0.222 1(2)	−0.182 3(2)	0.169 1(2)
P(2)	0.021 75(6)	−0.181 25(6)	−0.167 42(7)	O(8)	−0.068 9(2)	−0.291 5(2)	0.104 4(2)
P(3)	0.090 94(6)	−0.049 01(6)	0.264 50(8)	O(1W)	0.315 2(2)	0.148 6(2)	0.241 6(3)
P(4)	−0.102 61(6)	−0.174 58(6)	0.123 72(7)	O(2W)	−0.008 0(3)	0.355 3(2)	0.481 4(3)
O(1)	0.302 9(2)	−0.088 2(2)	0.088 7(2)	O(3W)	0.873 5(3)	0.459 8(2)	−0.008 0(4)
O(2)	0.269 6(2)	−0.018 7(2)	−0.156 0(2)	C(1)	0.150 3(2)	−0.184 4(2)	−0.071 2(3)
O(3)	−0.018 1(2)	−0.303 4(2)	−0.149 5(2)	C(2)	−0.033 2(2)	−0.120 2(3)	0.280 4(3)

Table 3. Co-ordinates for $K_4[Pt_2\{\mu\text{-}CH_2[P(O)OH]_2\}_4Cl_2]\cdot 8H_2O$

Atom	x	y	z	Atom	x	y	z
Pt	0.064 61(2)	0.004 68(2)	0.373 47(1)	O(4)	−0.093 4(4)	0.344 7(3)	0.610 3(4)
K(1)	0.095 4(2)	0.676 6(1)	0.102 6(1)	O(5)	−0.152 4(4)	0.330 1(4)	0.199 3(4)
K(2)	0.381 1(2)	0.166 9(1)	0.846 0(1)	O(6)	−0.179 4(4)	0.114 9(4)	0.142 5(3)
Cl(1)	0.183 3(2)	−0.003 0(1)	0.153 7(1)	O(7)	−0.317 4(4)	0.316 4(4)	0.521 9(4)
P(1)	0.173 3(1)	0.213 4(1)	0.338 5(1)	O(8)	−0.435 1(4)	0.093 7(4)	0.628 6(3)
P(2)	0.034 0(1)	0.199 3(1)	0.624 2(1)	C(1)	0.176 0(6)	0.257 5(5)	0.489 6(5)
P(3)	−0.153 2(1)	0.162 9(1)	0.262 3(1)	C(2)	−0.322 4(5)	0.148 1(5)	0.373 6(4)
P(4)	−0.295 9(1)	0.151 6(1)	0.537 1(1)	O(1W)	0.457 6(5)	0.435 6(4)	0.692 0(4)
O(1)	0.338 7(4)	0.185 5(4)	0.284 0(3)	O(2W)	0.178 4(5)	0.367 2(4)	0.949 2(4)
O(2)	0.087 3(4)	0.362 6(4)	0.237 3(4)	O(3W)	0.478 4(5)	0.856 1(4)	0.941 4(4)
O(3)	0.109 7(4)	0.163 6(3)	0.755 5(3)	O(4W)	0.393 7(6)	0.525 1(6)	0.111 9(5)

synthetic procedure. The yellow phosphorescent rhombohedral crystal was mounted in a sealed capillary tube. Intensity data were collected on an Enraf-Nonius CAD4 diffractometer equipped with Mo-K_α radiation (λ = 0.710 73 Å) and a graphite monochromator by ω–2θ scans of variable rate designed to yield $\sigma(I) = 0.02I$ for all observable data. A maximum of 120 s was placed on the scan time for weak reflections. The crystal data and final residuals are collected in Table 1. One quarter-sphere of data was collected and corrected for L_p, background, and absorption effects. The absorption correction was made using ψ scans. Data having $I > 3\sigma(I)$ were used in the refinement. The structure was solved by the heavy-atom method. The anion lies on a centre of symmetry. All atoms were located on difference maps. The hydrogen atoms of the water molecules were not refined, the other hydrogen atoms were refined isotropically, and all non-hydrogen atoms were refined anisotropically.

A crystal of $K_4[Pt_2\{\mu\text{-}CH_2[P(O)OH]_2\}_4Cl_2]\cdot 8H_2O$ was grown by the slow reaction of the crystal of $K_4[Pt_2\{\mu\text{-}CH_2[P(O)OH]_2\}_4]\cdot 6H_2O$ with chloride ion and air in the mother-liquor from the synthesis reaction of this latter complex. Several months were required for this transformation. The red rhombohedral crystal which formed from the yellow crystals was mounted in a sealed capillary tube, and the data collected as before, except that one half-sphere of data was collected. The structure was solved by the heavy-atom method. All hydrogen atoms, except for those on one water molecule [O(4W)], were located but not refined.[9]

Scattering factors and anomalous dispersion coefficients, and computer programs used for the structure solutions, were part of a local package. Final atomic co-ordinates are given in Tables 2 and 3.

Simulation of N.M.R. Spectra.—Computer simulation is required to extract all non-proton coupling constants from the ^{31}P and ^{195}Pt n.m.r. spectra of the complexes $[Pt_2(pop)_4]^{4-}$, $[Pt_2(pop)_4X_2]^{4-}$, $[Pt_2(pcp)_4]^{4-}$, and $[Pt_2(pcp)_4X_2]^{4-}$, where X is a halide. The spectra of the pcp complexes were collected by selective decoupling of the methylenic protons, thereby simplifying the spectra and the spin system. Each complex is a mixture of three isotopomers: Pt_2, $Pt^{195}Pt$, and $^{195}Pt_2$. Since the natural abundance of ^{195}Pt is 33.7%, the relative amounts of these complexes are 0.438:0.448:0.114. The other isotopomers, all with $I = 0$, are ^{190}Pt (0.0127), ^{194}Pt (32.9), ^{196}Pt (25.3), and ^{198}Pt (7.21%). The Pt_2 complex, which represents a composite of isotopomers containing ^{190}Pt, ^{194}Pt, ^{196}Pt, and ^{198}Pt, is an A_8 spin system with eight chemically and magnetically equivalent nuclei. The $Pt^{195}Pt$ complex is a nine-spin $AA'A''A^{3'}XA^{4'}A^{5'}A^{6'}A^{7'}$ ($[A]_4[X][A']_4$) system with C_{4v} symmetry, and the $^{195}Pt_2$ complex is a ten-spin $AA'A''A^{3'}$-$XX'A^{4'}A^{5'}A^{6'}A^{7'}$ ($[A]_4[X]_2[A']_4$) system with D_{4h} symmetry, where A and A' designate chemically equivalent but magnetically non-equivalent phosphorus nuclei, and X designates the ^{195}Pt ($I = \frac{1}{2}$) nuclei. In this Haigh notation the subscript 4 corresponds to the C_4 symmetry element. Complex spin systems of such high multiplicity usually generate too many transitions for useful solutions to be obtained, but these complexes have such high symmetry that meaningful spectral simulations can be obtained from the experimental spectra. Of the available simulation programs, LAOCOON III is usually dimensioned for a smaller number of spins than is required to solve this problem, and NUMARIT is restricted to systems with two-fold rather than four-fold symmetry.[10] The spectra were therefore simulated using a combination of the PANIC and DSYMPLOT (development of SYMTRY) programs.[11,12] The DSYMPLOT program is ideal for such applications since it was written in a manner which exploits the molecular point-group symmetry of the molecule in the calculation. The program was modified by us to operate in FORTRAN IV(G1) with double-precision words on an IBM 3081GX computer controlled by MUSIC. The ten-spin system was treated in the more general C_{4h} symmetry, as no extra information is given using D_{4h} symmetry. We know of no other transition-metal complexes having nine or ten magnetically non-equivalent nuclei that have been successfully

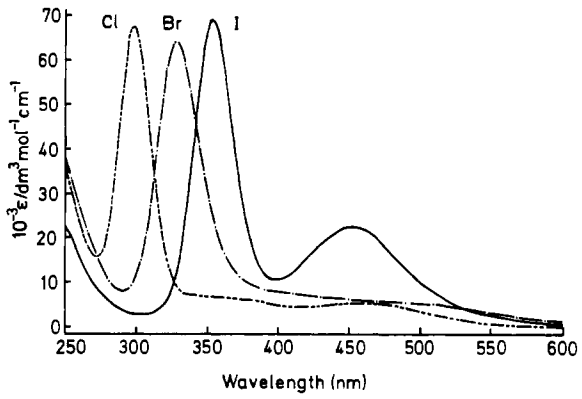

Figure 1. Electronic absorption spectra for $[Pt_2(pcp)_4X_2]^{4-}$ (X = Cl, Br, or I)

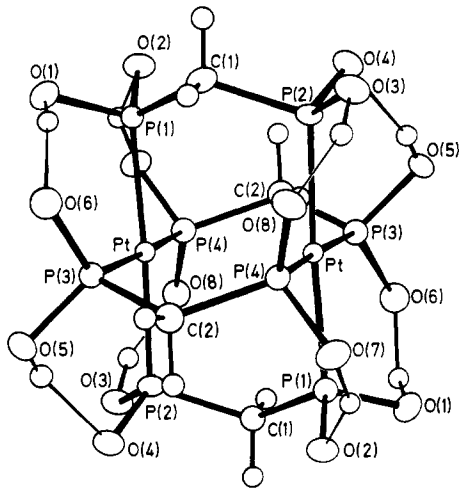

Figure 2. ORTEP representation of the anion in $K_4[Pt_2\{\mu\text{-}CH_2[P(O)OH]_2\}_4]\cdot 6H_2O$

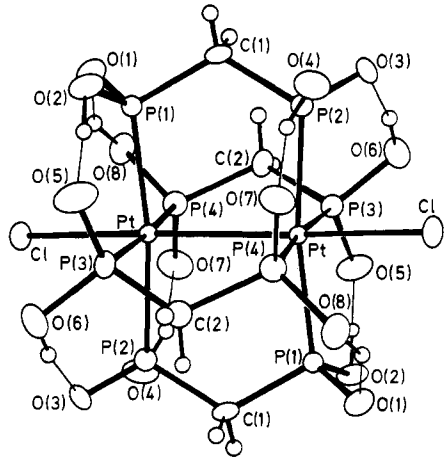

Figure 3. ORTEP representation of the anion in $K_4[Pt_2\{\mu\text{-}CH_2[P(O)OH]_2\}_4Cl_2]\cdot 8H_2O$

simulated. These compounds have five unique J(PP) couplings: $^2J(PP)_{cis}$, $^2J(PP)_{trans}$, $J(PP)_{syn}$, $J(PP)_{gauche}$, and $J(PP)_{anti}$. In addition there are couplings due to ^1J(PtP), ^2J(PtP), and ^1J(PtPt).

By approximating the spin systems as $[A_4][X][A'_4]$ and $[A_4][X]_2[A'_4]$ which contain three and four magnetically non-equivalent groups of nuclei, respectively, the major features of the ^{195}Pt spectra can be simulated using PANIC, but several of the smaller transitions are absent in the fits. The X part of the $[A_4][X][A'_4]$ spectrum is a quintet of quintets characterized by ^1J(PtP) and ^2J(PtP). If J(AA') is ignored, then the effective frequency of these lines ν_{Pt} relative to the chemical shift of platinum will depend only on the spin of the phosphorus [equation (1)], where m_n is the spin of one of the phosphorus nuclei. If $m_a = m_1 + m_2 + m_3 + m_4$, and $m_b = m_5 + m_6 + m_7 + m_8$, then ν_{Pt} is given by equation (2), where m_a and m_b

$$\nu_{Pt} = {}^1J(PtP)(m_1 + m_2 + m_3 + m_4) + {}^2J(PtP)(m_5 + m_6 + m_7 + m_8) \quad (1)$$

$$\nu_{Pt} = {}^1J(PtP)m_a + {}^2J(PtP)m_b \quad (2)$$

can be 2, 1, 0, −1, or −2. Since J(PP) is non-zero, some deviations in intensity and peak position from a perfectly symmetrical quintet of quintets is observed and the simulated spectrum is composed of some 900 non-degenerate lines. Of these lines, only about 100 have intensity greater than 1%.

The X part of the $[A_4][X]_2[A'_4]$ system is characterized by an additional coupling, ^1J(PtPt), which can be extracted from the ^{195}Pt n.m.r. spectrum by PANIC. This system can be viewed as a composite of ab pairs produced by coupling of 'pairs of lines' of equal intensity in the $[A_4][X][A'_4]$ system by ^1J(PtPt). For any orientation of the ^{31}P spins, $^{195}Pt_a$ with effective frequency ν_a couple to $^{195}Pt_b$ with effective frequency ν_b [equations (3) and (4)] with coupling constant ^1J(PtPt), to

$$\nu_a = {}^1J(PtP)(m_a) + {}^2J(PtP)(m_b) \quad (3)$$

$$\nu_b = {}^1J(PtP)(m_b) + {}^2J(PtP)(m_a) \quad (4)$$

produce an ab pair. This process is repeated for all possible combinations of m_a and m_b to give 15 pairs of lines that can couple. These ten ab pairs and five single lines ($\nu_a = \nu_b$) are listed in the Appendix, along with their relative intensities. The total simulated ^{195}Pt n.m.r. spectrum was formed by adding the X parts of the $[A_4][X][A'_4]$ and $[A_4][X]_2[A'_4]$ systems in the ratio 44.8:22.8. In the diplatinum(III) complexes the ratio ^1J(PtPt)/J(PP) is large and PANIC gives acceptable simulations. For the diplatinum(II) compounds, however, this ratio is much smaller and the $[A_4]$ approximation cannot be used in place of the full $[A]_4$ simulation. The program DSYMPLOT was used successfully to simulate all the spectral features in the diplatinum-(II) and -(III) complexes, including the small transitions not accounted for by the PANIC simulations.

By the effective frequency (chemical shift) method[13] the A part of the $[A]_4[X][A']_4$ system is split into two separate $[A]_4[B]_4$ sub-spectra. When ^{195}Pt has spin + $\frac{1}{2}$, the effective chemical shift of the four 'A' phosphorus atoms directly bonded to this platinum is moved to $\frac{1}{2}[^1J(PtP)]$ from the eight-spin $[A_8]$ frequency. The effective chemical shift of the four 'B' phosphorus nuclei bonded to the other platinum is moved to $\frac{1}{2}[^2J(PtP)]$. These groups then couple to form one sub-spectrum. The other $[A]_4[B]_4$ sub-system occurs when ^{195}Pt has spin $-\frac{1}{2}$,then the effective chemical shifts are $-\frac{1}{2}[^1J(PtP)]$ and $-\frac{1}{2}[^2J(PtP)]$. Since the B parts of these sub-spectra overlap in the centre of the ^{31}P spectra, the A part was simulated by DSYMPLOT in order to extract $J(PP)_{syn}$, $J(PP)_{anti}$, $J(PP)_{gauche}$, $^2J(PP)_{cis}$, and $^2J(PP)_{trans}$. The coupling $^2J(PtP)_{trans}$ was taken as positive; initial values for $^2J(PP)_{trans}$ and $^2J(PP)_{cis}$ were +550 and −25 Hz, respectively. The vector

Table 4. Bond distances (Å) and angles (°) for $K_4[Pt_2\{\mu\text{-}CH_2[P(O)OH]_2\}_4]\cdot 6H_2O$

Pt–Pt	2.980 1(2)	P(2)–O(3)	1.613(2)	C(1)–H(11)	0.747(36)	P(2)–C(1)	1.824(3)
Pt–P(1)	2.330(1)	P(2)–O(4)	1.532(2)	C(1)–H(12)	1.025(31)	O(7)–H(70)	1.160(59)
Pt–P(2)	2.332(1)	P(3)–C(2)	1.823(3)	C(2)–H(21)	1.093(45)	O(3)–H(30)	0.964(36)
Pt–P(3)	2.328(1)	P(3)–O(5)	1.602(2)	C(2)–H(22)	0.914(35)	O(8)–H(30)	1.624(36)
Pt–P(4)	2.320(1)	P(4)–C(2)	1.820(3)	O(1)–H(10)	0.939(32)	P(3)–O(6)	1.530(2)
P(1)–C(1)	1.814(3)	P(4)–O(7)	1.607(2)	O(6)–H(10)	1.692(32)	O(4)–H(50)	1.931(37)
P(1)–O(1)	1.611(2)	P(4)–O(8)	1.529(2)	O(2)–H(70)	1.507(59)	O(5)–H(50)	0.691(35)
P(1)–O(2)	1.529(2)						
Pt–Pt–P(1)	92.14(2)	P(3)–Pt–P(4)	175.95(2)	Pt–P(3)–C(2)	113.37(9)	C(1)–P(1)–O(2)	108.07(12)
Pt–Pt–P(2)	90.89(2)	Pt–P(1)–C(1)	110.25(8)	Pt–P(3)–O(5)	110.91(8)	O(1)–P(1)–O(2)	105.78(11)
Pt–Pt–P(3)	90.75(2)	Pt–P(1)–O(1)	110.02(8)	Pt–P(3)–O(6)	117.32(8)	C(1)–P(2)–O(3)	101.75(12)
Pt–Pt–P(4)	93.29(2)	Pt–P(1)–O(2)	118.86(8)	Pt–P(4)–C(2)	111.52(9)	C(1)–P(2)–O(4)	107.72(11)
P(1)–Pt–P(2)	176.97(2)	Pt–P(2)–C(1)	111.19(9)	Pt–P(4)–O(7)	110.67(8)	O(3)–P(2)–O(4)	106.81(10)
P(1)–Pt–P(3)	89.56(2)	Pt–P(2)–O(3)	110.96(7)	Pt–P(4)–O(8)	117.20(7)	C(2)–P(3)–O(5)	102.25(12)
P(1)–Pt–P(4)	89.95(2)	Pt–P(2)–O(4)	117.20(8)	P(1)–C(1)–P(2)	117.05(14)	C(2)–P(3)–O(6)	107.89(12)
P(2)–Pt–P(3)	90.42(2)	C(2)–P(4)–O(7)	102.58(11)	P(3)–C(2)–P(4)	119.28(14)	O(5)–P(3)–O(6)	103.63(11)
P(2)–Pt–P(4)	89.85(2)	C(2)–P(4)–O(8)	109.09(12)	C(1)–P(1)–O(1)	102.56(12)	O(7)–P(4)–O(8)	104.59(11)

Table 5. Bond distances (Å) and angles (°) for $K_4[Pt_2\{\mu\text{-}CH_2[P(O)OH]_2\}_4Cl_2]\cdot 8H_2O$

Pt–Pt	2.750 0(3)	P(1)–C(1)	1.812(4)	P(4)–C(2)	1.804(4)	O(4)–O(7)	2.499(4)
Pt–P(1)	2.386(1)	P(1)–O(1)	1.533(3)	P(4)–O(7)	1.525(3)	P(2)–O(4)	1.569(3)
Pt–P(2)	2.385(1)	P(1)–O(2)	1.562(3)	P(4)–O(8)	1.581(3)	P(3)–C(2)	1.808(4)
Pt–P(3)	2.365(1)	P(2)–C(1)	1.817(4)	O(1)–O(8)	2.507(4)	P(3)–O(5)	1.530(3)
Pt–P(4)	2.376(1)	P(2)–O(3)	1.538(3)	O(2)–O(5)	2.413(4)	P(3)–O(6)	1.575(3)
Pt–Cl	2.442(1)			O(3)–O(6)	2.489(4)		
Pt–Pt–P(1)	94.80(2)	P(3)–Pt–P(4)	174.17(3)	C(1)–P(1)–O(1)	105.20(19)	C(2)–P(4)–O(7)	106.45(18)
Pt–Pt–P(2)	93.14(2)	P(1)–Pt–Cl	87.74(3)	C(1)–P(1)–O(2)	104.48(19)	Pt–P(1)–C(1)	114.59(15)
Pt–Pt–P(3)	93.73(2)	P(2)–Pt–Cl	84.38(3)	O(1)–P(1)–O(2)	107.72(19)	C(2)–P(4)–O(8)	103.59(19)
Pt–Pt–P(4)	92.08(2)	Pt–P(1)–O(1)	111.36(13)	C(1)–P(2)–O(3)	104.77(18)	O(7)–P(4)–O(8)	107.31(17)
Pt–Pt–Cl	176.66(3)	P(3)–Pt–Cl	88.34(4)	C(1)–P(2)–O(4)	105.07(19)	Pt–P(1)–O(2)	112.87(13)
P(1)–Pt–P(2)	171.95(3)	P(4)–Pt–Cl	85.88(4)	O(3)–P(2)–O(4)	106.48(17)	Pt–P(2)–C(1)	116.22(14)
P(1)–Pt–P(3)	91.91(4)	Pt–P(2)–O(3)	111.86(12)	C(2)–P(3)–O(5)	106.82(19)	Pt–P(2)–O(4)	111.68(12)
P(1)–Pt–P(4)	87.08(4)	Pt–P(3)–O(2)	111.78(15)	C(2)–P(3)–O(6)	105.24(19)	Pt–P(4)–C(2)	113.05(14)
P(2)–Pt–P(3)	86.24(4)	P(3)–C(2)–P(4)	111.79(23)	O(5)–P(3)–O(6)	105.29(19)	P(1)–C(1)–P(2)	116.22(22)
P(2)–Pt–P(4)	93.98(4)						

sum $J(PP)_{syn} + 2[J(PP)_{gauche}] + {}^3J(PP)_{anti}$ was found to be just slightly larger than the separation of the dominant outer lines of the satellites. In the $[A_4][X][A'_4]$ and $[A_4][X]_2[A'_4]$ systems, $J(PP)$ is set equal to the separation of the dominant lines, in effect setting the *syn*, *gauche*, and *anti* couplings equal. The coupling $J(PP)_{syn}$ cannot be distinguished from $J(PP)_{anti}$ by the computer, and was assigned to the larger of the two couplings.

Simulation of the A part of the $[A]_4[X]_2[A']_4$ system revealed two lines of approximately one-half total intensity which were separated by exactly ${}^1J(PtP) + {}^2J(PtP)$. The positions of the less intense lines were found to be dependent on ${}^1J(PtPt)$, and non-iterative simulation gave reliable values for this coupling constant. The program DSYMPLOT is absolutely necessary for spectral simulation of the diplatinum(II) complexes $[Pt_2(pop)_4]^{4-}$ and $[Pt_2(pcp)_4]^{4-}$, in which the $[A_4][X]_2[A'_4]$ approximation doesn't work.

Results and Discussion

The complex $K_4[Pt_2(pcp)_4]$ has been prepared by treating a citrate (or acetate) buffer solution of potassium tetrachloroplatinate with H_2pcp and heating the solution at 103 °C for 72 h [equation (5)]. The product slowly crystallizes from the

$$2\,K_2[PtCl_4] + 4\,pcp^{2-} \longrightarrow K_4[Pt_2(pcp)_4] + 8\,Cl^- \quad (5)$$

reaction mixture. The complex in aqueous solution shows characteristic absorption bands at 382 (ε 2.9 × 10^4) and 470 nm (ε 142 $dm^3\ mol^{-1}\ cm^{-1}$), and an emission band centred at 510 nm. Aqueous solutions of $[Pt_2(pcp)_4]^{4-}$ or $[Pt_2(pop)_4]^{4-}$ react with halogens X_2 to give the axially substituted diplatinum(III) complexes $[Pt_2(pcp)_4X_2]^{4-}$ or $[Pt_2(pop)_4X_2]^{4-}$ (X = Cl, Br, or I) [equation (6)], which can be precipitated from solution by

$$[Pt_2(pcp)_4]^{4-} + X_2 \longrightarrow [Pt_2(pcp)_4X_2]^{4-} \quad (6)$$

the addition of methanol. For the pcp series of complexes, excess of halogen cannot be used in reaction (6) or decomposition of the product complex to unidentified compounds occurs. These diplatinum(III) complexes have been characterized by a combination of u.v.–visible and ${}^{31}P\text{-}\{{}^1H\}$ and ${}^{195}Pt\text{-}\{{}^1H\}$ n.m.r. spectroscopy,[3] although $K_4[Pt_2(pcp)_4Cl_2]\cdot 8H_2O$ has been structurally verified by *X*-ray crystallography. In aqueous solution, the complexes $[Pt_2(pcp)_4X_2]^{4-}$ show absorbances due to $X \rightarrow Pt^{III}$ ligand to metal charge-transfer transitions at 298 (ε 6.7 × 10^4) for X = Cl, 326 (ε 6.4 × 10^4) for X = Br, and both 354 (ε 7 × 10^4) and 454 nm (ε 2.2 × 10^4 $dm^3\ mol^{-1}\ cm^{-1}$) for X = I (Figure 1). Under photochemical conditions (λ > 335 nm) halide-ion interchange can be used to interconvert between $[Pt_2(pcp)_4X_2]^{4-}$ and $[Pt_2(pcp)_4Y_2]^{4-}$ [equation (7);

$$[Pt_2(pcp)_4X_2]^{4-} + 2\,Y^- \longrightarrow [Pt_2(pcp)_4Y_2]^{4-} + 2\,X^- \quad (7)$$

$X \neq Y$ = Cl, Br, or I], a reaction which has also been described for $[Pt_2(pop)_4X_2]^{4-}$.[14]

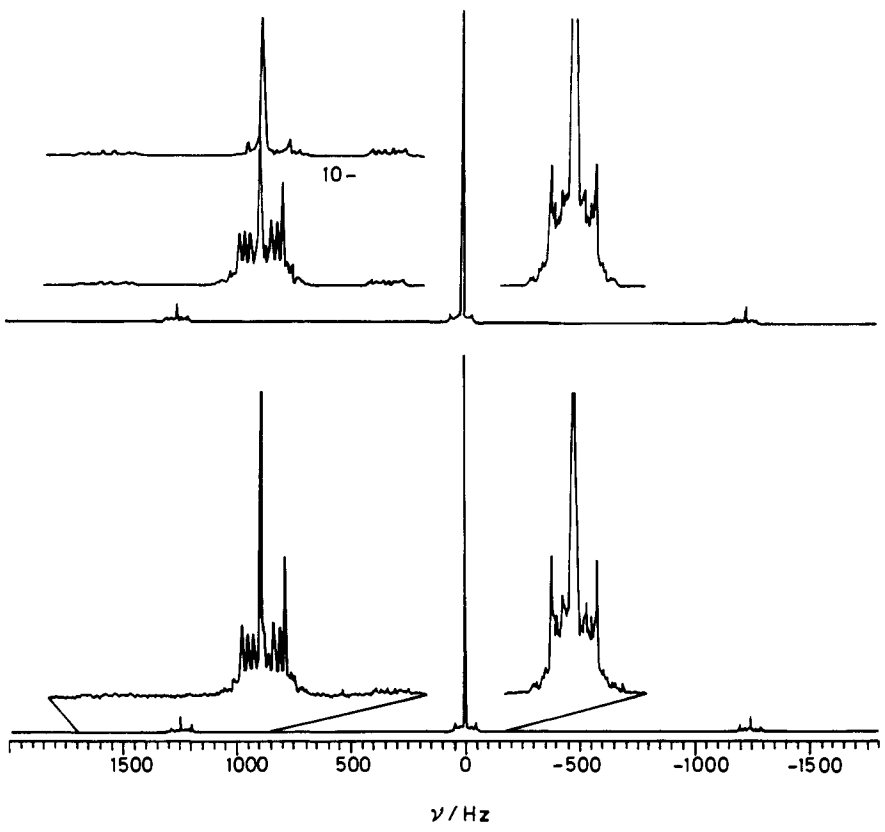

Figure 4. Experimental and simulated (eight- plus nine- plus ten-spin) ^{31}P n.m.r. spectrum of $[Pt_2(pcp)_4]^{4-}$. The section marked 10- is for the ten-spin isotopomer only

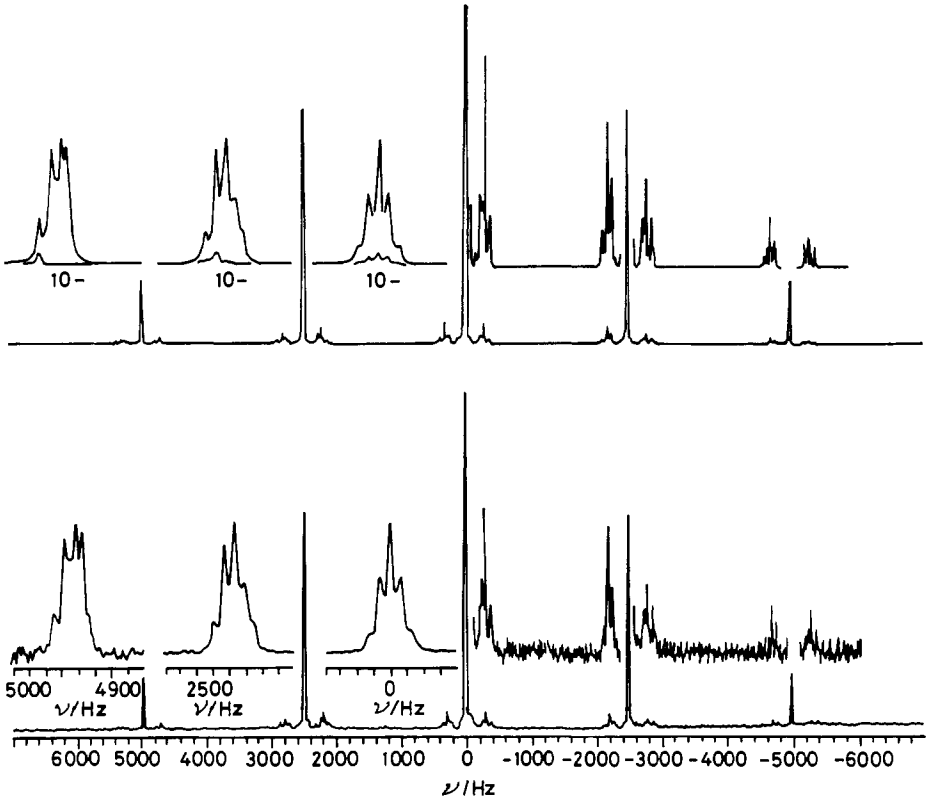

Figure 5. Experimental and simulated (nine- plus ten-spin) ^{195}Pt n.m.r. spectrum of $[Pt_2(pcp)_4]^{4-}$. The section marked 10- is for the ten-spin isotopomer only

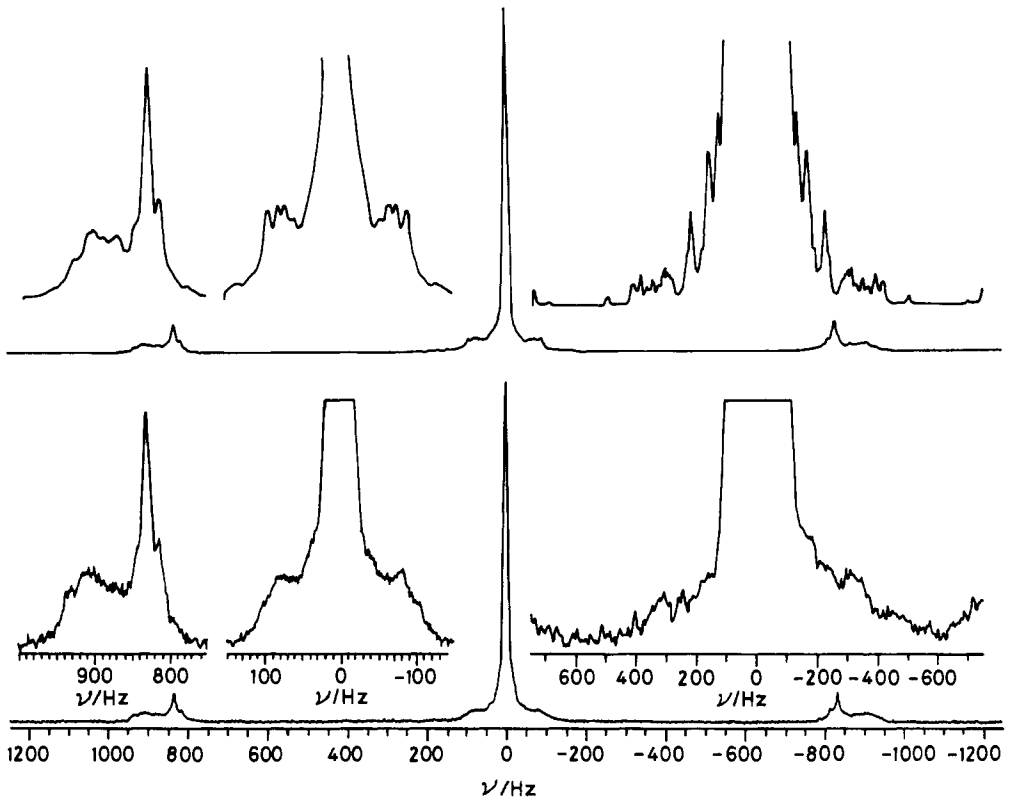

Figure 6. Experimental and simulated ^{31}P n.m.r. spectrum of $[Pt_2(pcp)_4Cl_2]^{4-}$

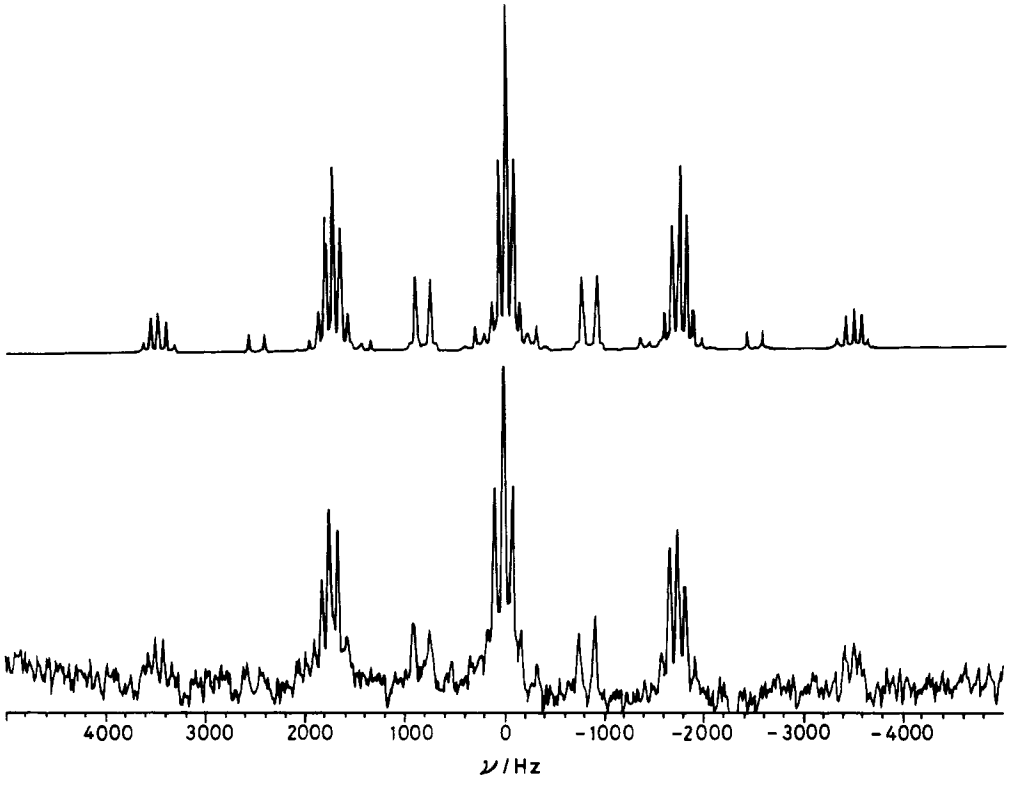

Figure 7. Experimental and simulated ^{195}Pt n.m.r. spectrum of $[Pt_2(pcp)_4Cl_2]^{4-}$

Table 6. N.m.r. chemical shift and coupling constant data

Complex	δ(Pt)	δ(P)	δ(H)	^1J(PtPt)[a]	^1J(PtP)[b]	^2J(PtP)	J(PP) *cis*	J(PP) *trans*[b]	J(PP) *syn*	J(PP) *anti*	J(PP) *gauche*
$[Pt_2(pop)_4]^{4-}$	−5 139	69.4	—	±800	+3 095	−18	−33	+460	+33	−1	+2
$[Pt_2(pcp)_4]^{4-}$	−5 037	96.8	2.83	+594	+2 485	+9.8	−32.6	+470	+91	−3	0
$[Pt_2(pop)_4Cl_2]^{4-}$	−4 236	28.0	—	±8 080	+2 170	−85.5	−25	+560	+49	+30	−2
$[Pt_2(pcp)_4Cl_2]^{4-}$	−4 049	58.8	3.58	±10 500	+1 743	−74.5	−35	+550	+106	+11	−1
$[Pt_2(pop)_4Br_2]^{4-}$	−4 544	24.0	—	±7 900	+2 185	−84	−25	+560	+42.5	+22	+4
$[Pt_2(pcp)_4Br_2]^{4-}$	−4 298	54.0	3.71	±9 500	+1 755	−74.2	−25	+565	+102	+15	0
$[Pt_2(pop)_4I_2]^{4-}$	−5 103	18.0	—	±6 990	+2 200	−75.5	−29	+560	+42	+22	+4
$[Pt_2(pcp)_4I_2]^{4-}$	−4 749	45.6	4.01	±8 300	+1 773	−67.2	−25	+540	+100	+13	0

[a] The sign of ^1J(PtPt) in $[Pt_2(pcp)_4]^{4-}$ is the same as that of $^2J(PP)_{trans}$. [b] The signs of ^1J(PtP) and $^2J(PP)_{trans}$ are assumed to be positive.

Structures of $K_4[Pt_2(pcp)_4]\cdot 6H_2O$ *and* $K_4[Pt_2(pcp)_4Cl_2]\cdot 8H_2O$.—The *X*-ray crystal structures of these compounds confirm that the complexes adopt a 'lantern' structure with the phosphorus ligating atoms in equatorial planes. Selected bond distances and angles are collected in Tables 4 and 5, and ORTEP representations of the anions are shown in Figures 2 and 3. The compound $K_4[Pt_2(pcp)_4]\cdot 6H_2O$ [diplatinum(II)] has a Pt–Pt separation of 2.980 1(2) Å, whereas $K_4[Pt_2(pcp)_4Cl_2]\cdot 8H_2O$ [diplatinum(III)] has a Pt–Pt distance of 2.750 0(3) Å. This shortening of the Pt–Pt distance on converting from diplatinum(II) into diplatinum(III) is characteristic of intermetallic bond formation. The conversion of Pt^{II}_2 into Pt^{III}_2 is accompanied by a decrease in the P(1)–C(1)–P(2) and P(3)–C(2)–P(4) angles from 117.05(14) and 119.28(14)° to 116.22(22) and 111.79(23)°. The bending about the bridge angle is not the only conformational change which occurs, since there is also a slight distortion of the platinum atoms out of the P_4 planes. Thus in diplatinum(II) we find the Pt–Pt–P angles to be 91.77(2)[119]°, whereas in diplatinum(III) the corresponding angles are 93.44(2)[98]°. The Pt–P distances in diplatinum(III) are slightly, but probably not significantly, longer than in diplatinum(II): 2.378(1)[8] as against 2.323(1)[5] Å. The Pt–Cl distances [2.442(1) Å] are long because of the high *trans* influence of the Pt^{III}_2 bond.[4] The other ligand distances and angles remain relatively constant between Pt^{II}_2 and Pt^{III}_2. Each structure shows alternating short and long P=O and P–O distances {1.530(2)[1] and 1.608(2)[5] Å in Pt^{II}_2, and 1.532(3)[19] and 1.572(3)[7] Å in Pt^{III}_2}, and a short hydrogen-bonded O–H · · · O separation between oxygens of 2.578(3)[24] and 2.477(4)[37] Å in Pt^{II}_2 and Pt^{III}_2 respectively. The numbers in square brackets are the root-mean-square deviations of the different individual values. These structural features correlate closely with those observed in the tetrakis-μ-diphosphonito series of complexes.[4]

Phosphorus-31 and ^{195}*Pt N.M.R. Spectroscopy*.—The ^{31}P and ^{195}Pt n.m.r. spectra of the series of complexes $[Pt_2(pcp)_4]^{4-}$, $[Pt_2(pcp)_4X_2]^{4-}$, $[Pt_2(pop)_4]^{4-}$, and $[Pt_2(pop)_4X_2]^{4-}$ (X = Cl, Br, or I) show both similarities and differences between the two sets of spectra. All spectra have been measured in D_2O solvent, and for the pcp complexes the band multiplicities are reduced by broad-band proton decoupling of the methylenic hydrogens. In all cases the ^{31}P spectra are dominated by a single peak, but additional resonances are observed due to coupling with ^{195}Pt in the isotopomers which are both singly and doubly labelled with this isotope ($I = \frac{1}{2}$, abundance = 33.7%). The analysis of the spectra is complicated by the fact that although the phosphorus nuclei are chemically equivalent, they are magnetically inequivalent. Complete spectral analysis requires simulation as overlapping peaks resulting from a mixture of eight-, nine-, and ten-spin systems. Experimental and simulated ^{31}P-{^{1}H} and ^{195}Pt-{^{1}H} n.m.r. spectra for $[Pt_2(pcp)_4]^{4-}$ and $[Pt_2(pcp)_4X_2]^{4-}$ (X = Cl, Br, or I) using DSYMPLOT are shown in Figures 4—11, and the calculated chemical shift and coupling constant data are collected in Table 6 for these and the analogous pop compounds.

Several spectral features are immediately apparent. These are that the values of ^1J(PtP) in the diplatinum(II) complexes are in the region of 3 000 Hz, and the same coupling constants in the diplatinum(III) complexes are approximately 2 200 Hz. Secondly, it is clear from the ^{31}P chemical shift data collected in Table 6 that there is an upfield shift in δ(P) of approximately 40—50 p.p.m. on converting from diplatinum-(II) into -(III). Both the ^{31}P and ^{195}Pt chemical shifts in these complexes are expected to be dominated by the paramagnetic term in the Ramsey equation (8),[15–17] where $\Delta E_A = E(^1A_{2g}) - E(^1A_{1g})$ and $\Delta E_E = E(^1E_g) - E(^1A_{1g})$, and the coupling constants ^1J(PtP) can be understood on the basis of the Pople and Santry

$$\sigma_p \approx \langle r^{-3}\rangle C^2_{a_{1g}}(2C^2_{a_{2u}}\Delta E_A^{-1} + C^2_{e_g}DE_E^{-1}) \quad (8)$$

$$^1J_{A-B} = -\delta_A\delta_B\cdot\frac{h}{2\pi}\cdot\frac{256}{9}\pi^2\beta^2|S_A(0)|^2|S_B(0)|^2 \sum_i^{occ}\sum_j^{unocc}(^3\Delta E_{i\rightarrow j})^{-1}C_iS_AC_jS_AC_jS_BC_iS_B \quad (9)$$

equation (9).[18] The decrease in ^1J(PtP) of approximately 800 Hz on converting the Pt^{II}_2 into the Pt^{III}_2 complexes correlates with a corresponding increase in ^1J(PtPt) of up to 9 700 Hz between these groups of complexes. These coupling constant differences can be explained on the basis of the Pople–Santry equation. The increase in ^1J(PtPt) of the Pt^{III}_2 complexes over the Pt^{II}_2 complexes correlates with the formation of a diplatinum(III) bond in $[Pt_2(pop)_4X_2]^{4-}$ and $[Pt_2(pcp)_4X_2]^{4-}$. Increased *s*-orbital character between platinum atoms in the formation of a Pt^{III}_2 bond will result in a correspondingly decreased *s*-orbital character in the Pt–P bonds, and hence in reduced values of ^1J(PtP). The direction and magnitude of Δ^1J(PtP) closely corresponds with that (1 342 Hz) found between *trans*-$[PtCl_2(PEt_3)_2]$ and *trans*-$[PtCl_4(PEt_3)_2]$, where the formation of σ bonds to two additional chlorines decreases the *s*-orbital participation in each Pt–P bond.[19] Equation (8) for the calculation of the paramagnetic shift parameter (σ_p) has been developed for a monomeric complex with D_{4h} symmetry. Since our Pt^{II}_2 and Pt^{III}_2 complexes also approximate to this symmetry, it is useful to check whether the ^{31}P and ^{195}Pt chemical shifts show a similar correlation with the electronic transitions between the molecular orbitals of our bimetallic complexes. In Figure 12 we show that there is a reasonably linear correlation between both δ(P) and δ(Pt) and λ (nm) for the Pt^{III}_2 complexes of both pop and pcp with changing axial

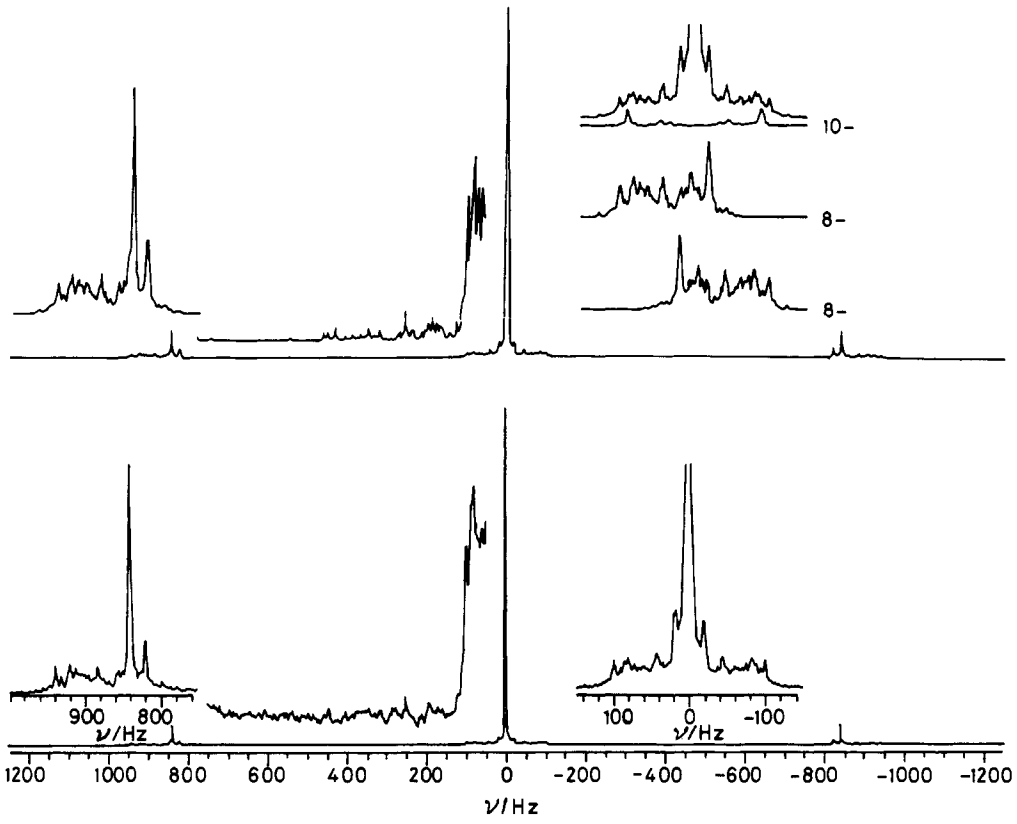

Figure 8. Experimental and simulated (nine- plus ten-spin) ^{31}P n.m.r. spectrum of $[Pt_2(pcp)_4Br_2]^{4-}$. The sections marked 8- are the results of using the effective frequency method; that marked 10- is for the ten-spin isotopomer only

ligands X. The slope in Figure 12 shows the dominance of the orbital mixing coefficients over the chemical shifts.

The large values of ^1J(PtPt) in the Pt^{III}_2 complexes is indicative of a homometallic bond between platinum atoms. Although no linear correlation exists between ^1J(Pt–Pt) and the Pt–Pt bond strength, a large value of ^1J(PtPt) is accepted as being diagnostic of significant intermetallic bonding.[20–24] Our measured values in the 7 000—11 000 Hz range are indeed among the largest known for ^1J(PtPt).

Spectral simulation of the ^{31}P and ^{195}Pt n.m.r. spectra allows the magnitudes of the five different J(PP) couplings to be evaluated. Before the data can be used for interpretive purposes, we need to address the question of coupling pathways between the magnetically inequivalent phosphorus nuclei. Grim *et al.*[25] and others[26] have shown that in metal–diphosphine chelate complexes the coupling between the phosphorus nuclei L and L′ can either be through the bonds to platinum, or across the ligand backbone. For these pop and pcp complexes we also have the possibility that the couplings J(PP) can involve communication through the platinum centres, through the ligand bridge, or a combination of both. The three types of J(PP) dihedral couplings across the two platinum centres are given in equations (10)—(12). The factors of two in equations (11) and (12) reflect the presence of two degenerate coupling routes: ^4J(PPtPCP) and ^4J(PCPPtP).

$$^2J(PP)_{syn} = {}^2J(PCP) + {}^3J(PPtPtP)_{0°} \quad (10)$$

$$^3J(PP)_{gauche} = 2[{}^4J(PPtPCP)_{90°}] + {}^3J(PPtPtP)_{90°} \quad (11)$$

$$^3J(PP)_{anti} = 2[{}^4J(PPtPCP)_{180°}] + {}^3J(PPtPtP)_{180°} \quad (12)$$

The largest ^2J(PP) values are the *trans* couplings across a single platinum centre. The values in the Pt^{III}_2 complexes are slightly larger than those found in the Pt^{II}_2 complexes, but all values range between 460 and 565 Hz. The magnitude of $^2J(PP)_{cis}$ across a single platinum centre is some 20-fold smaller than $^2J(PP)_{trans}$, and is also opposite in sign. The $J(PP)_{syn}$ coupling constants are the largest values of J(PP) across the two platinum centres. The values range from +33 to +106 Hz, and are slightly larger in the Pt^{III}_2 than in the Pt^{II}_2 complexes. Nevertheless, it is significant that these values are much larger than that in $CH_2[PH(O)OH]_2$ itself, where from the linewidths in the ^{31}P n.m.r. spectrum of $CH_2[PH(O)OH][PD(O)OH]$ we can estimate that ^2J(PCP) is less than 3 Hz.[6]

The J(PP) coupling across the two platinum(III) centres reasonably follows a Karplus-type relationship for the magnitudes of the coupling constants. The values of $J(PP)_{syn}$ and $J(PP)_{anti}$ with dihedral angles of 0 and 180° are relatively large (+15 to +102 Hz), whereas the values of $J(PP)_{gauche}$, which has a dihedral angle of 90°, are small (0 to +4 Hz). This angular dependence of J(PP) with dihedral angle correlates with an analogous relationship of J(HH).[27] The diplatinum(II) complexes $[Pt_2(pcp)_4]^{4-}$ and $[Pt_2(pop)_4]^{4-}$ show very small values for both $J(PP)_{anti}$ and $J(PP)_{gauche}$. Indeed, the magnitude of $J(PP)_{anti}$ can be explained on the basis of there being no significant intermetallic bonding between the diplatinum(II) centres. For the diplatinum(III) complexes, which have an intermetallic bond, the value of $J(PP)_{anti}$ is larger by approximately 15—20 Hz than the corresponding value for the diplatinum(II) complexes. Inspection of the values of $J(PP)_{syn}$ between the Pt^{II}_2 and the Pt^{III}_2 complexes reveals that $J(PP)_{syn}$ is some 10—20 Hz larger in the latter complexes, but that in all

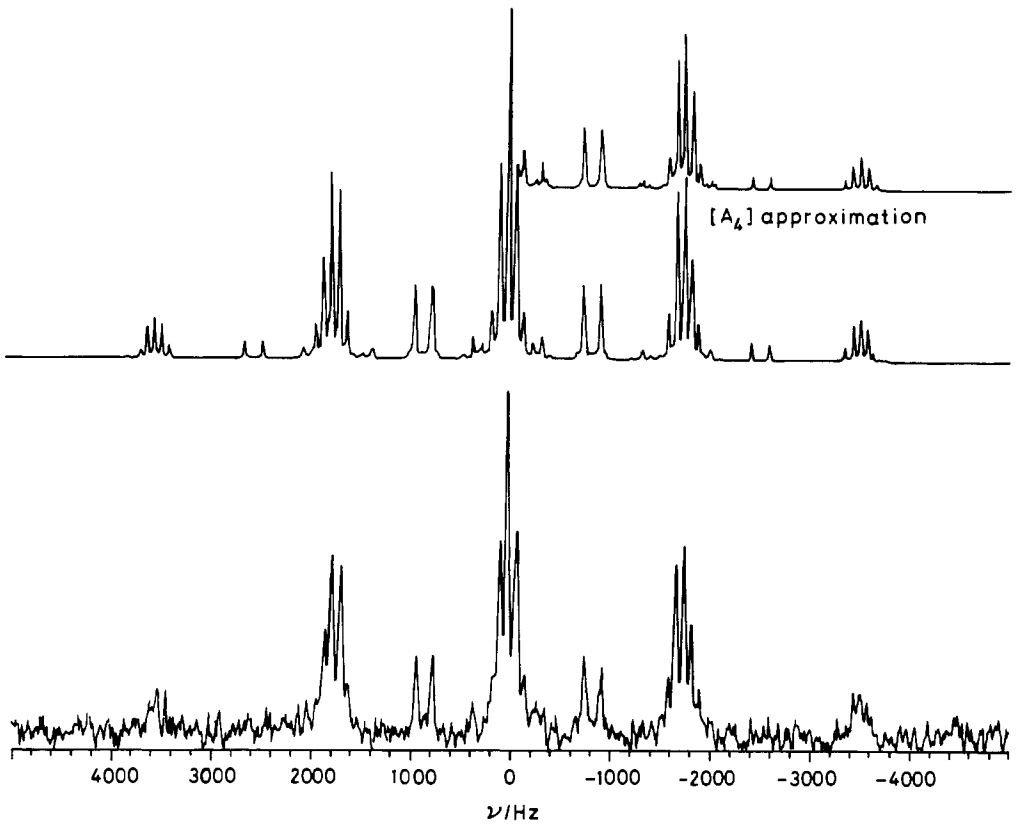

Figure 9. Experimental and simulated ^{195}Pt n.m.r. spectrum of $[Pt_2(pcp)_4Br_2]^{4-}$

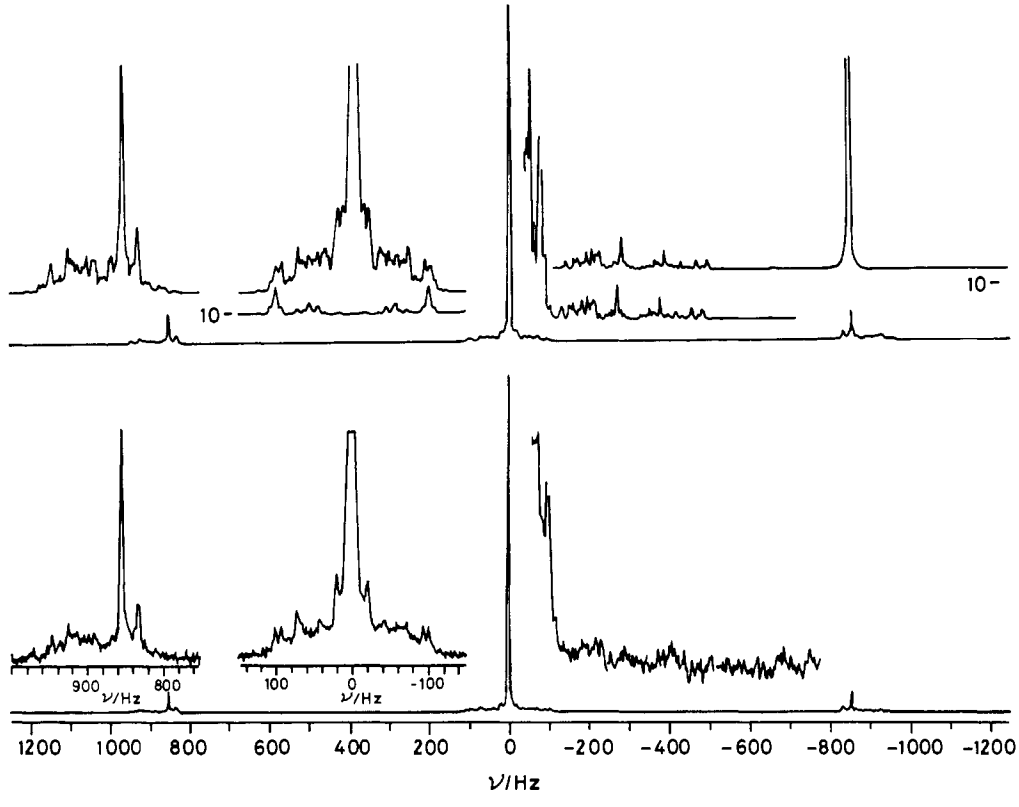

Figure 10. Experimental and simulated (nine- plus ten-spin) ^{31}P n.m.r. spectrum of $[Pt_2(pcp)_4I_2]^{4-}$. The section marked 10- is for the ten-spin isotopomer only

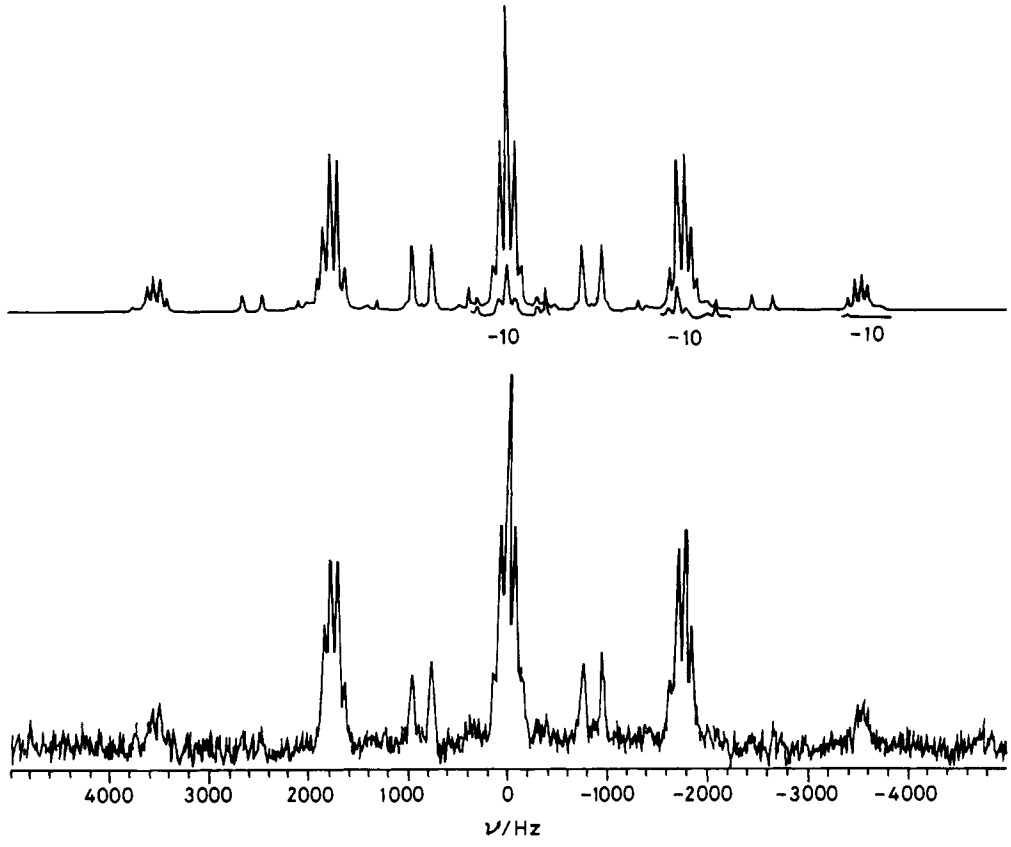

Figure 11. Experimental and simulated (nine- plus ten-spin) ^{195}Pt n.m.r. spectrum of $[Pt_2(pcp)_4I_2]^{4-}$. The section marked 10- is for the ten-spin isotopomer only

eight cases the value of $J(PP)_{syn}$ is greater than $J(PP)_{anti}$, and especially for the Pt^{II}_2 complexes. The larger value of $J(PP)_{syn}$ in the complexes $[Pt_2(pcp)_4]^{4-}$ and $[Pt_2(pop)_4]^{4-}$ is due primarily to coupling across the ligand binding atom, and therefore the component ^2J(PCP) or ^2J(POP) is larger than the $^3J(PPtPtP)_0$ coupling across the metal centres.

Appendix

The combinations of $\nu(Pt_a)$ and $\nu(Pt_b)$ with their relative weights are given below, where ^1J and ^2J refer to ^nJ(PtP).

Sub-spectrum type	Weight	$\nu(Pt_a)$	$\nu(Pt_b)$
a_2	1	$2(^1J) + 2(^2J)$	$2(^1J) + 2(^2J)$
ab	8	$2(^1J) + 1(^2J)$	$1(^1J) + 2(^2J)$
ab	12	$2(^1J) + 0(^2J)$	$0(^1J) + 2(^2J)$
ab	8	$2(^1J) - 1(^2J)$	$-1(^1J) + 2(^2J)$
ab	2	$2(^1J) - 2(^2J)$	$-2(^1J) + 2(^2J)$
a_2	16	$1(^1J) + 1(^2J)$	$1(^1J) + 1(^2J)$
ab	48	$1(^1J) + 0(^2J)$	$0(^1J) + 1(^2J)$
ab	32	$1(^1J) - 1(^2J)$	$-1(^1J) + 1(^2J)$
ab	8	$1(^1J) - 2(^2J)$	$-2(^1J) + 1(^2J)$
a_2	36	$0(^1J) + 0(^2J)$	$0(^1J) + 0(^2J)$
ab	48	$0(^1J) - 1(^2J)$	$-1(^1J) + 0(^2J)$
ab	12	$0(^1J) - 2(^2J)$	$-2(^1J) + 0(^2J)$
a_2	16	$-1(^1J) - 1(^2J)$	$-1(^1J) - 1(^2J)$
ab	8	$-1(^1J) - 2(^2J)$	$-2(^1J) - 1(^2J)$
a_2	1	$-2(^1J) - 2(^2J)$	$-2(^1J) - 2(^2J)$

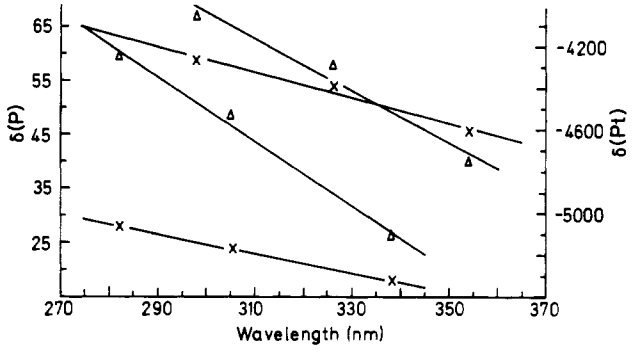

Figure 12. Plot of δ against wavelength for the $[Pt_2(pcp)_4X_2]^{4-}$ and $[Pt_2(pop)_4X_2]^{4-}$ complexes. The ordinates correspond to δ(P) (×) and δ(Pt) (△)

Acknowledgements

We are grateful to the donors of the Petroleum Research Fund, administered by the American Chemical Society, for support of this research. We thank Mr. D. Appel (Washington State University) for assistance with n.m.r. measurements on the Nicolet NT 200, and Professor Hagele for a copy of his DSYMPLOT n.m.r. program and for his initial assistance with its use.

References

1 R. P. Sperline, M. K. Dickson, and D. M. Roundhill, *J. Chem. Soc., Chem. Commun.*, 1977, 62.

2 M. A. F. Dos Remedios Pinto, P. J. Sadler, S. Neidle, M. R. Sanderson, A. Subbiah, and R. J. Kuroda, *J. Chem. Soc., Chem. Commun.*, 1980, 13.
3 C. M. Che, W. P. Schaefer, H. B. Gray, M. K. Dickson, P. B. Stein, and D. M. Roundhill, *J. Am. Chem. Soc.*, 1982, **104**, 4253.
4 K. A. Alexander, S. A. Bryan, F. R. Fronczek, W. C. Fultz, A. L. Rheingold, D. M. Roundhill, P. Stein, and S. F. Watkins, *Inorg. Chem.*, 1985, **24**, 2803.
5 P. Stein, M. K. Dickson, and D. M. Roundhill, *J. Am. Chem. Soc.*, 1983, **105**, 3489.
6 C. King and D. M. Roundhill, *Inorg. Chem.*, 1986, **25**, 1290.
7 C. King, R. A. Auerbach, F. R. Fronczek, and D. M. Roundhill, *J. Am. Chem. Soc.*, 1986, **108**, 5626.
8 K. A. Alexander, S. A. Bryan, M. K. Dickson, D. Hedden, and D. M. Roundhill, *Inorg. Synth.*, 1986, **24**, 211.
9 D. T. Cromer and J. T. Waber, 'International Tables for *X*-Ray Crystallography,' Kynoch Press, Birmingham, 1974, vol. 4, Tables 2.2B and 2.3.1; B. A. Frenze and Y. Okaya, 'Enraf-Nonius Structure Determination Package,' Enraf-Nonius, Delft, Holland, 1980.
10 A. R. Quirt and J. S. Martin, *J. Magn. Reson.*, 1971, **5**, 318.
11 PANIC 83.3004, 'Aspect 3000 NMR Software Manual,' Bruker Spectrospin, Karlsruhe, W. Germany, 1985.
12 V. Lueg and G. Hägele, *J. Magn. Reson.*, 1977, **26**, 505.
13 E. O. Bishop, *Annu. Rev. N.M.R. Spectrosc.*, 1968, **1**, 92.
14 S. A. Bryan, M. K. Dickson, and D. M. Roundhill, *J. Am. Chem. Soc.*, 1984, **106**, 1882.
15 N. F. Ramsey, *Phys. Rev.*, 1950, **78**, 699.
16 P. L. Goggin, R. J. Goodfellow, S. R. Haddock, B. F. Taylor, and I. R. H. Marshall, *J. Chem. Soc., Dalton Trans.*, 1976, 459.
17 P. S. Pregosin, *Coord. Chem. Rev.*, 1982, **44**, 247.
18 J. F. Nixon and A. Pidcock, *Annu. Rev. N.M.R. Spectrosc.*, 1969, **2**, 345.
19 D. W. W. Anderson, E. A. V. Ebsworth, and D. W. H. Rankin, *J. Chem. Soc., Dalton Trans.*, 1973, 2370.
20 P. S. Pregosin, *Annu. Rep. N.M.R. Spectrosc.*, 1986, **17**, 285.
21 A. Zschunke, H. Meyer, I. Heidlas, B. Messbauer, B. Walther, and H. D. Schädler, *Z. Anorg. Allg. Chem.*, 1983, **504**, 117.
22 J. J. Dechter, *Prog. Inorg. Chem.*, 1985, **33**, 393.
23 N. M. Boag, J. Browning, C. Crocker, P. L. Goggin, R. J. Goodfellow, M. Murray, and J. L. Spencer, *J. Chem. Res.*, 1978, (*S*) 228.
24 T. G. Appleton, J. R. Hall, D. W. Neale, and S. F. Ralph, *Inorg. Chim. Acta*, 1983, **77**, L149.
25 S. O. Grim, R. C. Barth, J. D. Mitchell, and J. D. Gaudis, *Inorg. Chem.*, 1977, **16**, 1776.
26 I. J. Colquhoun and W. McFarlane, *J. Chem. Res.*, 1978, (*S*) 368.
27 M. Karplus, *J. Chem. Phys.*, 1959, **30**, 11.

Received 16*th December* 1986; *Paper* 6/2428